Mon. Not. R. Astron. Soc. **362,** 966–974 (2005) doi:10.1111/j.1365-2966.2005.09369.x

# The radio structure of S5 1803+784

S. Britzen,[1,2,3⋆] A. Witzel,[1] T. P. Krichbaum,[1] T. Beckert,[1] R. M. Campbell,[4] C. Schalinski[5,6] and J. Campbell[7]

[1]*Max-Planck-Institut für Radioastronomie, Auf dem Hügel 69, D-53121 Bonn, Germany*
[2]*ASTRON, Netherlands Foundation for Research in Astronomy, Oude Hoogeveensedijk 4, PO Box 2, NL-7990 AA Dwingeloo, the Netherlands*
[3]*Landessternwarte, Königstuhl, D-69117 Heidelberg, Germany*
[4]*Joint Institute for VLBI in Europe, Oude Hoogeveensedijk 4, NL-7991 PD Dwingeloo, the Netherlands*
[5]*OHB-System AG, Universitätsallee 27–29, D-28359 Bremen, Germany*
[6]*ARCSPACE – Aerospace Research Consulting, Space Science & Technology, Kötnermoor 16, D-27442 Gnarrenburg, Germany*
[7]*Geodätisches Institut der Universität Bonn, Nussallee 17, D-53115 Bonn, Germany*

Accepted 2005 June 27. Received 2005 June 27; in original form 2005 May 30

**ABSTRACT**

The BL Lacertae object S5 1803+784 has been monitored with very long baseline interferometry at $\lambda = 3.6$ cm in 43 epochs between 1986.21 and 1993.95. The motivation of this work is to obtain statistically meaningful data with which to study the short-term structural variability in the source on monthly time-scales. We present a detailed analysis of the structural evolution seen in the milliarcsecond-scale jet by way of model-fitting results. Within the simplest identification scenario, the jet can be described as a bent chain of seven jet components within 0.2- and 3-mas separation from the core. New components seem to emerge almost regularly (every 2 yr) from the core. Three jet components approach the brightest and so-called 'stationary' component (at ∼1.4 mas at 8.4 GHz) with apparent superluminal motion of 8–11$c$. In this paper, we show that the 'stationary' component (under the assumption that this is the brightest jet component in each epoch) oscillates, and we discuss several possible explanations. We show that a reconfinement shock can easily reproduce the observed most recent oscillation of the 'stationary' component. We present evidence that the average jet ridge line is significantly curved and discuss the possibility that the jet components follow a helically bent path.

**Key words:** techniques: interferometric – BL Lacertae objects: individual: S5 1803+784 – radio continuum: galaxies.

## 1 INTRODUCTION

With a time sampling of up to one observation per month, it is possible to determine the trajectories and velocities of very long baseline interferometry (VLBI) jet components with an accuracy sufficient to trace the complex motion patterns seen in an increasing number of radio sources (Krichbaum et al. 1994a; Zensus 1997). Previous VLBI-monitoring data sometimes suffered from non-unique cross-identifications of VLBI components visible in maps obtained at different observing epochs, particularly if these components were moving faster than a few tenths of a milliarcsecond per year or travelling along bent or accelerated jets. The probability of such misidentifications is clearly reduced in densely sampled monitoring data, e.g. the geodetic data base, which besides the *X*-band observations analysed here, also provides *S*-band observations.

⋆E-mail: sbritzen@mpifr-bonn.mpg.de

Geodetic VLBI observations of quasars and BL Lacertae objects are designed to determine earth rotation parameters and geophysical crust motions, but they also provide a powerful data base for astrophysical investigations of source structures and their variability on milliarcsecond scales. Continuous monitoring of quasars started in the late 1970s and since then various observing programmes have gathered simultaneous dual-frequency (8.4 and 2.3 GHz) data over various time-scales. Advantageously, the observational sampling can be quite short, as in the case of International Radio Interferometric Surveying (IRIS) and IRIS–South (IRIS-S) campaigns where monthly data are taken (e.g. Schuh 1989).

The astrophysical potential of this data base has only been partly exploited until now. Because the accuracy of baseline and earth-rotation parameter determinations has reached a limit where source-structure contributions have become significant, there is substantial interest to monitor and eventually correct for the source-structure effects. The effects of source structure on group delays, which form the fundamental observable in geodetic VLBI experiments, have been investigated by Tang & Rönnäng (1988), Ulvestad (1988) and

Charlot (1990a). Previous papers have reported on the astronomical investigation of geodetic VLBI data and presented maps and model fits (e.g. Schalinski 1985; Tang, Rönnäng & Baath 1987; Schalinski et al. 1988a; Tang & Rönnäng 1988; Tang, Rönnäng & Baath 1989; Charlot 1990b, 1992; Tateyama et al. 2002).

## 2 THE VLBI JET OF S5 1803+784

S5 1803+784 is a BL Lac object with a redshift of $z = 0.68$ (Lawrence et al. 1986; Stickel, Fried & Kühr 1993) and particularly luminous emission lines (Lawrence et al. 1986). As an intraday variable, it also shows rapid flux-density variations in the optical and radio regimes (Wagner & Witzel 1995), on time-scales as short as 50 min in the optical (Wagner et al. 1990).

VLBI observations by Witzel and collaborators (e.g. Witzel et al. 1988) at different radio wavelengths reveal the complex morphology of the milliarcsecond-scale jet of this source. As a member of the complete S5 sample of 13 flat-spectrum radio sources (Witzel 1987), S5 1803+784 has been observed repeatedly at many frequencies and angular resolutions since the late 1970s (e.g. Eckart et al. 1986; Eckart, Witzel & Biermann 1987; Witzel et al. 1988). High-frequency VLBI observations of S5 1803+784 at 22 and 43 GHz monitor the motion of jet components located at smaller core separations ($r < 1.4$ mas; Krichbaum et al. 1993). These inner jet components move superluminally with expansion rates of $0.14 \pm 0.04$ and $0.07 \pm 0.05$ mas yr$^{-1}$, with possibly variable angular speeds (0.02–0.28 mas yr$^{-1}$) along a curved path, suggesting helical motion (Krichbaum 1990; Krichbaum et al. 1994b; Steffen et al. 1995; Steffen 1997). The discovery of superluminal motion in S5 1803+784 solved the X-ray discrepancy that had persisted for many years (Biermann et al. 1992). Such curved jet morphology is found also at larger core separations from VLBI-maps obtained at 3.6 cm (Britzen & Krichbaum 1995; Britzen 2002), at 6 cm (Britzen et al. 2005a) and at 18 cm (Britzen et al. 2005b).

On mas-scales, the source shows a pronounced jet with prominent jet components located at relative core separations of 1.4, 5 and 12 mas (Eckart et al. 1986). Geodetic and astronomical VLBI data gathered between 1979 and 1985 show that the component located at 1.4 mas is apparently stationary (Schalinski 1985; Schalinski et al. 1988a,b; Schalinski 1990). This finding has been confirmed in geodetic *X*-band observations between 1983 and 1987 (Schalinski et al. 1988b), as well as in 5-GHz VLBI observations between 1979 and 1985 ($0.00 \pm 0.07$ mas yr$^{-1}$, Witzel et al. 1988). Several authors confirm this constant separation (e.g. Cawthorne et al. 1993). Tateyama et al. (2002) however, based on 11 maps obtained at 8.3 GHz (geodetic VLBI observations) between 1988 and 1999, find three superluminal components moving with an expansion rate of 0.084 mas yr$^{-1}$ and one stationary component at 0.5 mas from the core. In their identification scenario the 'classical stationary' component at 1.4 mas is moving.

Another remarkable property of S5 1803+784 is the 76° difference in position angle between the parsec- and kiloparsec-scale jet. Observations at 1.5 GHz by Antonucci et al. (1986) found a 2-arcsec extension south-west of the core at position angle $\Theta \approx -120°$, as well as a weak (8.6 mJy) secondary component ∼45 arcsec away at position angle $\Theta \approx -166°$ south-south-west of the core, which is presumably physically related to the BL Lac object. A deep Very Large Array (VLA) B configuration image showing the large-scale structure of this object has also been presented by Cassaro et al. (1999). We describe the large-scale radio structure and the discovery of the transition region between the pc- and kpc-scale jet in Britzen et al. (2005b).

Preliminary results concerning the *X*-band VLBI monitoring have already been published in Britzen & Krichbaum (1995) and Britzen (2002). Other investigations of the structure of S5 1803+784 include, among others, Charlot (1990b), Fey, Clegg & Fomalont (1996), Kellermann, Vermeulen & Zensus (1998), Gabuzda (1999), Gabuzda & Cawthorne (2000) and Ros et al. (2000, 2001).

This is the first of a series of papers on the radio structure of S5 1803+784. In the second paper, we will concentrate on the description of the large-scale radio structure as seen in world array VLBI observations at 18 cm and in VLBI observations at 90 cm, especially the detection of the transition region between the pc- and kpc-scale jet (Britzen et al. 2005b).

## 3 OBSERVATIONS AND DATA REDUCTION

For our analysis, we preferentially investigated data originating in IRIS observations. This special campaign was undertaken to monitor UT1 and polar motion (Schuh 1989). The IRIS system has been routinely providing the *x* and *y* components of polar motion with an accuracy of better than ±1 mas and UT1 to ±0.05 ms.

In general about 15 sources, almost equally distributed in the sky, are observed between 10 and 15 times for about 3 to 7 min each during 24 h of observation. The data are recorded simultaneously at 2.3 and 8.4 GHz in Mk III mode. Correlation of all data sets is performed at the correlator of the Max-Planck-Institut für Radioastronomie in Bonn by the members of the Geodetic Institute of the University in Bonn.

The BL Lac object S5 1803+784 has belonged to the programme sources of this sample since at least 1983. In 1992.2, it was substituted by another source but then again inserted in 1994. Since 1994, its $u - v$ coverage has been reduced due to less observations per day.

From the total of all IRIS and IRIS-S VLBI observations performed on S5 1803+784, we selected 43 data sets observed at a frequency of 8.4 GHz with at least three participating antennas. A second criterion in this selection was achieving an almost uniform distribution of observations over the 6-yr observing period from 1986.21 to 1993.95.

Table 1 lists the participating antennas, their diameters, and introduces the abbreviations used in Table 2. The geodetic programme name, the epochs of the observations, the observing arrays and the number of scans, which might serve as an estimate for the $u - v$ coverage, are given in Table 2. Mapping and model fitting usually are based on data acquired during a full $u - v$ track of a source by a VLBI array and on complete calibration information for each

**Table 1.** Abbreviations for the telescopes in Table 2.

| Abbreviation | Antenna | Size (m) |
|---|---|---|
| WT | Wettzell, Germany | 20 |
| D | DSN-Madrid, Spain | 34 |
| ME | Medicina, Italy | 32 |
| N | Noto, Italy | 32 |
| O | Onsala, Sweden | 20 |
| M | Mojave, USA | 12 |
| HR | Ford Davis, USA | 25 |
| R | Richmond, USA | 16 |
| WS | Westford, USA | 18 |
| G | Gilcreek, USA | 25 |
| SE | Seshan, China | 25 |
| K | Kashima, Japan | 26 |
| HA | Hartebeesthoek, South-Africa | 26 |
| FO | Fortalezza, Brasilien | 14.2 |

**Table 2.** Details about the investigated epochs.

| Experiment | Epoch | Array | Number of scans |
|---|---|---|---|
| IRIS313 | 1986.21 | HR-O-WS-WT | 308 |
| IRIS316 | 1986.25 | HR-O-WS-WT | 404 |
| IRIS345 | 1986.65 | HR-O-WS-WT | 293 |
| IRIS359 | 1986.84 | HR-O-WS-WT | 348 |
| IRIS366 | 1986.94 | HR-O-WS-WT | 338 |
| IRIS390 | 1987.26 | HR-O-WS-WT | 373 |
| IRIS422 | 1987.70 | HR-O-WS-WT | 318 |
| IRIS457 | 1988.18 | HR-O-WS-WT | 455 |
| IRIS464 | 1988.28 | HR-O-WS-WT | 464 |
| IRIS468 | 1988.33 | HR-O-WS-WT | 443 |
| IRIS477 | 1988.46 | HR-O-WS-WT | 181 |
| IRIS492 | 1988.66 | HR-O-WS-WT | 251 |
| IRIS496 | 1988.72 | HR-O-WS-WT | 250 |
| IRIS506 | 1988.85 | HR-O-WS-WT | 262 |
| E.ATL-5 | 1988.95 | D-ME-O-WS-WT | 295 |
| IRIS513 | 1988.95 | HR-WS-WT | 78 |
| IRIS531 | 1989.20 | HR-O-WS-WT | 231 |
| IRIS540 | 1989.32 | HA-O-WS-WT | 259 |
| IRIS-P30 | 1989.72 | G-K-M | 69 |
| IRIS-S26 | 1990.08 | M-WS-WT | 37 |
| SHAWE90A | 1990.25 | K-SE-WT | 99 |
| IRIS-S29 | 1990.31 | M-WS-WT | 97 |
| IRIS-S30 | 1990.38 | M-WS-WT | 104 |
| IRIS-S31 | 1990.48 | M-WS-WT | 65 |
| IRIS-S32 | 1990.54 | M-WS-WT | 43 |
| IRIS-S33 | 1990.61 | M-WS-WT | 42 |
| IRIS-S34 | 1990.74 | M-WS-WT | 23 |
| IRIS-S37 | 1990.94 | HA-M-R-WS-WT | 65 |
| IRIS-S39 | 1991.12 | M-WS-WT | 100 |
| IRIS-S40 | 1991.23 | M-WS-WT | 103 |
| IRIS-S41 | 1991.31 | M-WS-WT | 106 |
| IRIS-S42 | 1991.34 | M-N-WS-WT | 43 |
| IRIS-S43 | 1991.44 | M-WS-WT | 89 |
| IRIS-S44 | 1991.54 | M-N-WS-WT | 127 |
| IRIS-S45 | 1991.59 | M-N-WS-WT | 148 |
| IRIS-S46 | 1991.67 | M-N-WS-WT | 123 |
| IRIS-S47 | 1991.82 | M-WS-WT | 131 |
| IRIS-S48 | 1991.86 | M-WS-WT | 130 |
| IRIS-S49 | 1991.94 | M-WS-WT | 110 |
| IRIS-S51 | 1992.15 | M-WS-WT | 111 |
| IRIS-S52 | 1992.19 | M-WS-WT | 104 |
| IRIS-S54 | 1992.34 | M-SE-WS-WT | 176 |
| IRIS-S73 | 1993.95 | HA-FO-WS-WT | 80 |

radio telescope. Although the $u - v$ coverage is sparse (though uniform across epochs) and gain curves, as well as simultaneous flux-density data, are not available in astrometric/geodetic experiments, it has been recently demonstrated that such experiments can provide valuable maps (Britzen et al. 1999, 2000). A careful and cautious calibration is indispensable for the reliability of the results.

The system temperatures and sensitivity at each radiotelescope were combined to produce correlated flux densities by the usual VLBI calibration scheme. For the initial amplitude calibration of the data, the sensitivity of each station was approximately estimated from the VLBI data acquired on 4C39.25. This source is included in the geodetic sample and its structural evolution at different frequencies is well known from astronomical observations (Marcaide et al. 1989; Alberdi et al. 1993a,b). After data export from the correlator, the data were transferred into the California Institute of Technology VLBI Reduction Program (CIT-package) and were analysed using the standard procedures provided within this package (Pearson 1991).

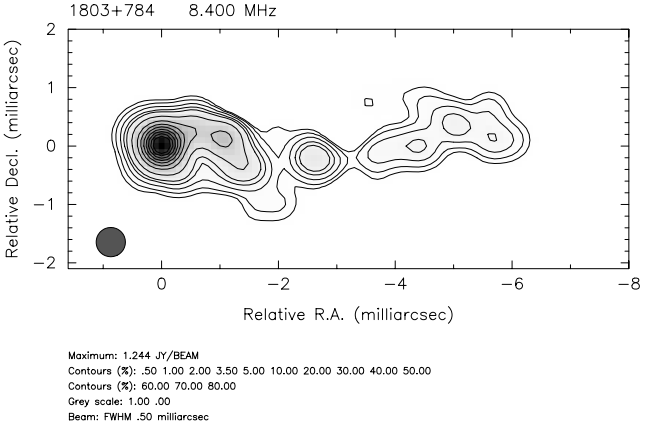


**Figure 1.** A CLEAN map of S5 1803+784 (epoch 1991.23) at 8.4 GHz is shown. The complex jet structure extends beyond the inner 3 mas discussed in detail in this paper. Components at larger core separations have not been considered further here.

The data analysis of each observation was done in several steps. Starting from a point-source model, we mapped the source using the standard phase self-calibration and CLEAN algorithms. In parallel, we fitted elliptical Gaussian components to the visibilities. Starting in each case from a single-component model, the agreement between model and data was improved by adding further components to the model. Depending on data quality and $u - v$ coverage, we obtained models with typically five to eight Gaussian components, providing final component parameters and error estimates for the individual jet components. Structure associated with all of the elliptical Gaussian model components was also seen in the CLEAN maps. The Gaussian parameters include flux density, position relative to the VLBI core, component size, axial ratio and orientation. The parameters obtained via model fitting are given in Britzen (1997). The values and errors of the parameters of the individual components were estimated from a comparison between alternative Gaussian component models fitted to the same data set and from a comparison between model fits and maps: as typical relative errors we obtained $\sim$20 per cent for the flux density, $\pm$0.15 mas for the relative core separation, $\sim$15 per cent for the component size and 5°–10° for the position angle relative to the core. Additionally, we calculated the parameter errors using the program ERRFIT, which is also implemented in and provided by the CIT-package. These errors seemed to be more realistic because the errors for each data set are calculated independently from all the others. We used these errors as plausible estimates of the real error in the diagrams presented below. We show a CLEAN map describing the complex jet structure of this source in more detail in Fig. 1. The jet of 1803 + 784 clearly reveals more jet components than discussed in this paper. In Fig. 2, we show the model-fit results for 40 epochs for the jet components within 3 mas of core separation. We have chosen to fold the model fits with a circular beam of 0.5-mas size. This simplifies a comparison of the results for the different epochs and reproduces the observational situation best with mostly circularly shaped beams of this size. The high declination of this source leads to almost circular beams, even in the extreme case of a purely east–west array.

## 4 RESULTS

Consistent with observations at other frequencies (Eckart et al. 1986, 1987; Schalinski et al. 1988b; Witzel et al. 1988), we obtain a

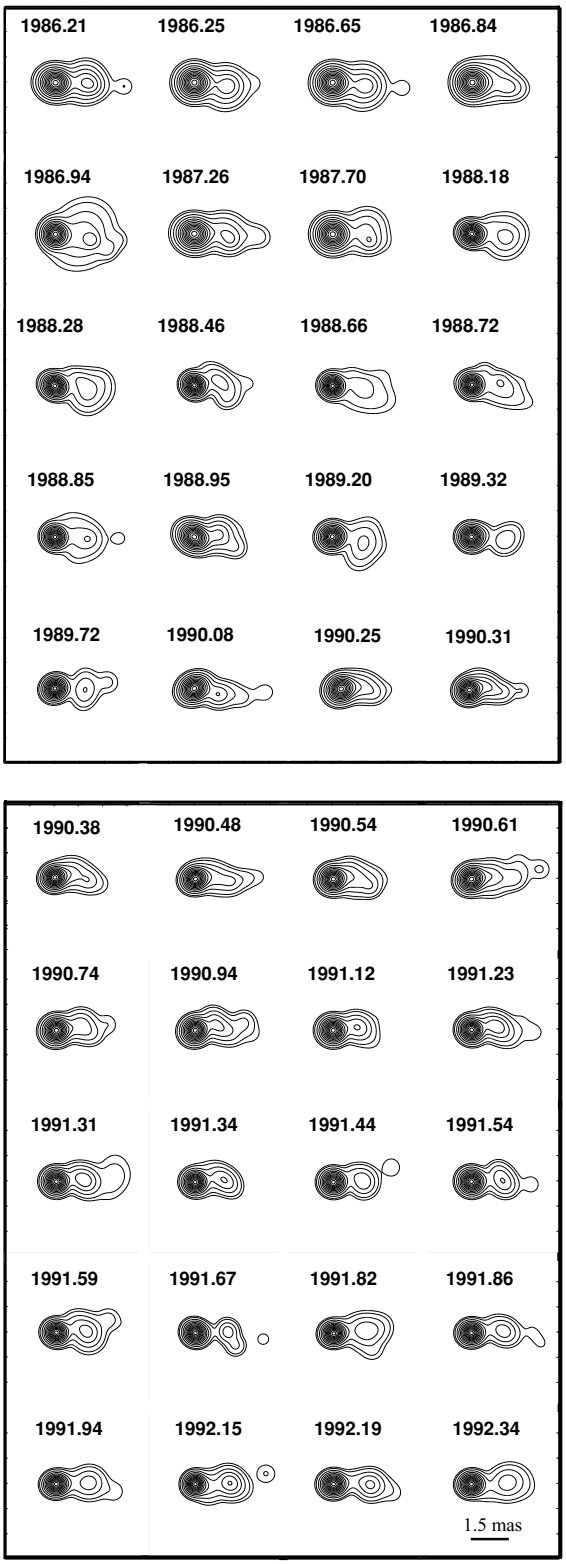


**Figure 2.** Model-fit results for S5 1803+784 for the time 1986.21–1992.34. Jet components within ∼3 m as core separation are shown. Details concerning the model-fit parameters are listed in Britzen (1997). The size of the circular beam is 0.5 mas.

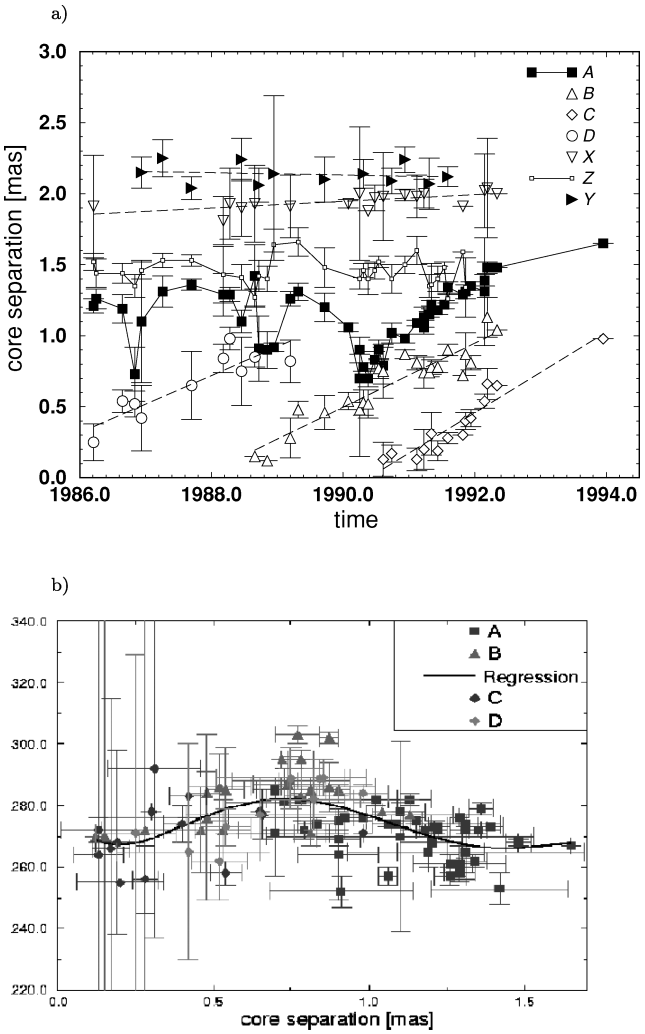


**Figure 3.** (a) The jet components in S5 1803+784 and the kinematics of their core separation as a function of time between 1986 and 1994. (b) The position angle distribution as a function of core separation. The brightest jet components A, B, C and D from 43 epochs are included. To guide the eye, we plot a least-squares fit of a sinusoid function to the data (solid line).

one-sided core-jet structure, consisting of seven components oriented mainly along a position angle of 270°.

The identification of the jet components was done in two steps. First, a component located at $r = 1.4$ mas could be identified as the so-called 'stationary' component (Schalinski et al. 1988b). We labelled this component A. The prominence of the flux density of the VLBI core and component A, which is about 5 times brighter than the remaining jet components individually, facilitated the second step of identifying the remaining jet components on the basis of their relative positions. In Fig. 2, we show the results of fitting Gaussian

**Table 3.** The linear regression coefficient, the standard error and the apparent velocity for each of the 'moving' components.

| Component | Proper motion (mas/year) | Stand. err. (mas/year) | $\beta_{\rm app}$ |
|---|---|---|---|
| B | 0.225 | 0.019 | $8.7c \pm 0.7c$ |
| C | 0.285 | 0.027 | $11.1c \pm 1.1c$ |
| D | 0.201 | 0.038 | $7.8c \pm 1.5c$ |

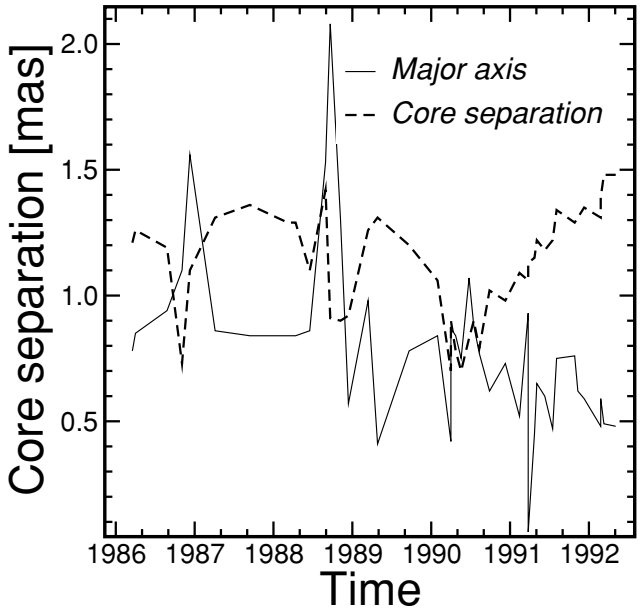


**Figure 4.** The evolution with time of the core separation (dashed line) and the size of the major axis (solid line) of the bright component A is shown.

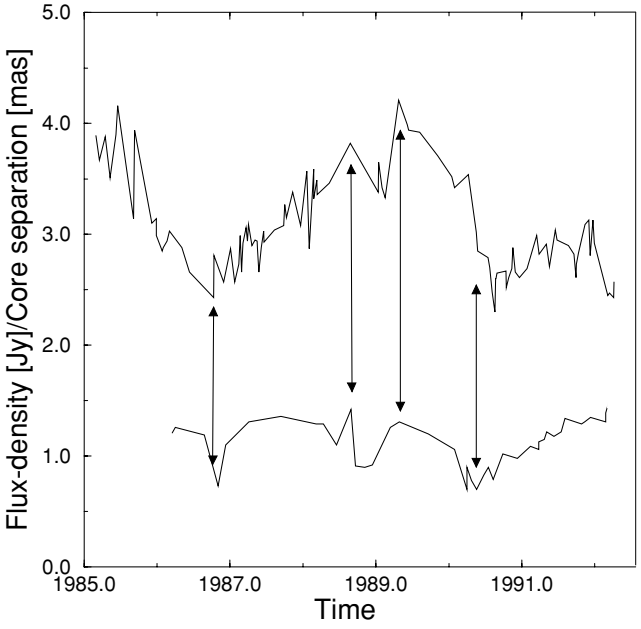


**Figure 5.** The core separation of component A (lower line) and the total flux density as observed by the Michigan monitoring programme at 8.4 GHz (upper line) as function of time.

models to the observed visibilities for 40 selected epochs (1986.21–1992.34) for the inner 3 mas from the core. Fig. 3(a) shows the core separation as a function of time for all seven jet components. Fig. 3(b) shows the position angle distribution as a function of the core separation (the 'path') for the brightest jet components A, B, C and D. The average position angle increases (starting at a core separation of ∼0.2 mas) and reaches a maximum at a core separation of 0.75 mas followed by a return to the original position angle at 1.5 mas. To calculate the apparent speeds (see Table 3), we did not take the curvature into account.

Three inner jet components B, C and D seem to separate from the core with apparent speeds of $\beta_{\rm app} = 8.7c \pm 0.7c$, $\beta_{\rm app} = 11.1c \pm 1.1c$ and $\beta_{\rm app} = 7.8c \pm 1.5c$, respectively, as listed in Table 3. We calculated the apparent velocities from the proper motions assuming cosmological parameters that were taken from the *WMAP* data (Spergel et al. 2003; $h = 0.71$, $\Omega_{\rm b}h^2 = 0.0224$, $\Omega_{\rm m}h^2 = 0.135$).

Adjacent to the bright component A, three much fainter components X, Y and Z can be found. Significant deviations from apparent stationarity is seen for component A, with its position shifting between $r \sim 0.7$ mas and $r \sim 1.5$ mas (see Fig. 3).

We can distinguish three 'core approaching events' (hereafter CAE) in Fig. 3. In the first two CAEs, the time A spends close to the core is very short, while the third CAE takes longer and is defined by many more epochs. A 'approaches' the core whenever a new component seems to just have emerged from the core or is going to emerge from the core. Component D is not seen any more after apparently reaching the same core separation as A, while component B can still be traced later on.

In Fig. 4, we compare the motion of component A with its major axis. From inspection of this figure, it is obvious that minima in core separation correlate with maxima of the major axis of this jet component, although the increase in the size of the major axis seems to trail slightly. The core separation of jet component A and the total flux density of S5 1803+784 (Aller, private communication) also show correlated behaviour: larger core separations seem to correlate with a larger total flux density (see Fig. 5). The flux density of component A alone instead shows some evidence for an anticorrelated behaviour: smaller core separations correlate with larger component flux densities (see Fig. 6b). The jet components B, C and D show almost constant flux densities with time, as seen in Figs 6(c)–(e). The flux-density stability of the components B, C and D is atypical because most jet components reveal an exponential decay in flux density with increasing core separation (e.g. Homan et al. 2002).

In Fig. 7, we present the motion parametrized in rectangular coordinates $X(t)$ and $Y(t)$. For components B, C, D and A, we derive a fit to the component offsets $X(t)$ and $Y(t)$ from the position of the core. The form of the fitting function is selected individually for each component and for each coordinate for each component in order to give the best representation of the data so the fits adequately represent the observed bends in the trajectories.

Based on the data presented in the previous sections, we can divide the jet components into two groups: (i) the inner jet components that have apparent superluminal, clearly outward directed motion; and (ii) the 'formerly stationary' component A that reveals CAEs. The jet component at even larger core separations (Z, $r \sim 1.5$ mas) seems to remain at the same core separation with some evidence for similar oscillatory behaviour as in A. Components X and Y show slight evidence for outward motion. However, because of the large position errors, the motion of these jet components is less well constrained. In Fig. 8, we plot X and Y with the same symbol to stress the possibility that these might belong to the same component.

## 5 DISCUSSION

The results presented above rely upon the simplest identification scenario where the brightest component in all epochs is identified with component A. Based upon these assumptions, justified by the fact that A has been found to be the dominant jet component in many previous observations (e.g. Schalinski et al. 1988b), we find

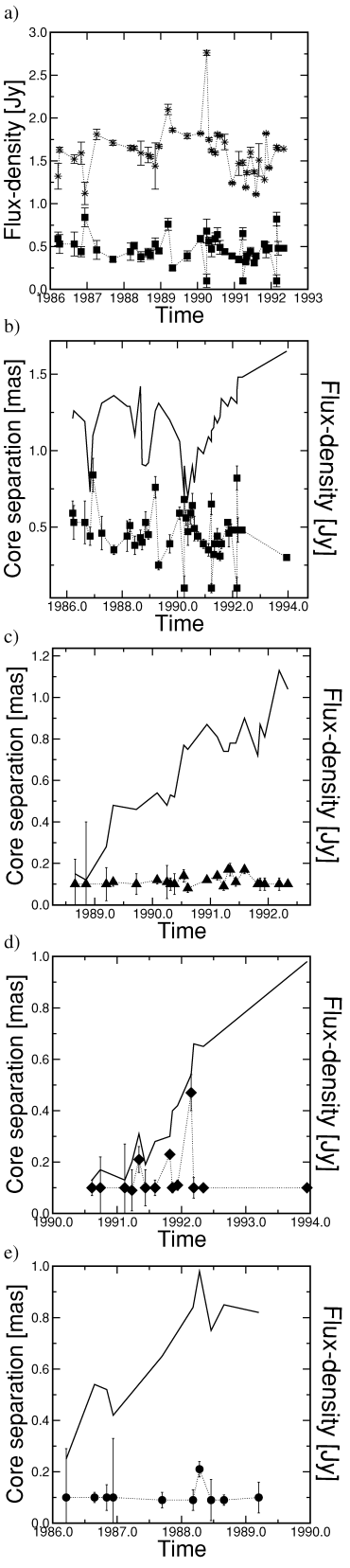


**Figure 6.** (a) The total source flux density of 1803+784 (stars) as well as the flux density of component A (black filled squares). (b–e) Both the core separation (solid black line) and the component VLBI flux density (dotted grey line) at 8.4 GHz of 1803+784 as a function of time for the individual jet components A to D, respectively.

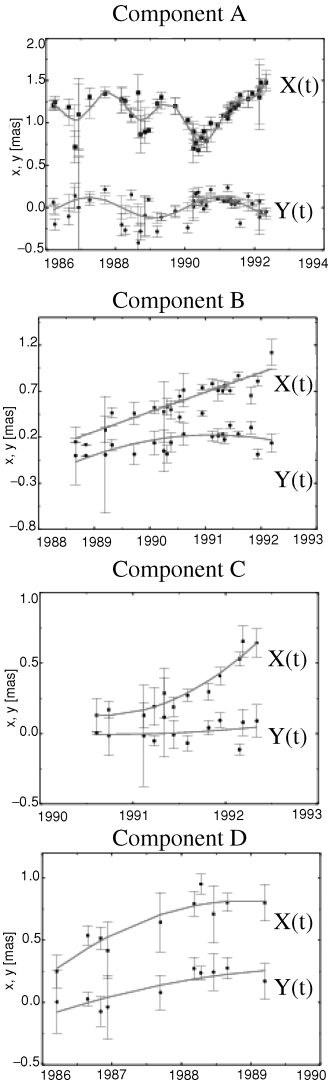


**Figure 7.** The motion parametrized in rectangular coordinates $X(t)$ ($X =$ west) and $Y(t)$ ($Y =$ north).

the coexistence of components that move superluminally and at least one component that oscillates or is stationary in the bent jet of S5 1803+784. The mean jet axis as defined by the brightest jet components A, B, C and D reveals significant curvature.

For several sources, coexistence of superluminal and stationary jet components has already been observed: for example, the superluminal motion of a component lying between stationary components in 4C 39.25 (Alberdi et al. 2000) and 3C 395 (Simon et al. 1988), or several superluminal components in 0735+178 (Gabuzda et al. 1994).

This coexistence of superluminally moving and stationary jet components can be explained within relativistic time-dependent hydrodynamical models (Agudo et al. 2001) as a result of the interaction of the superluminal component with the underlying jet. Multiple conical shocks form behind the main perturbation. Those appearing closer to the core could be identified as stationary components. 4C39.25 is the most prominent source known for the simultaneous existence of stationary and moving components. Alberdi et al. (2000) interpret the stationary feature in 4C39.25 as a bend in the jet trajectory in a plane different from the observers plane. The moving feature is according to them a shock turning around the bend. A

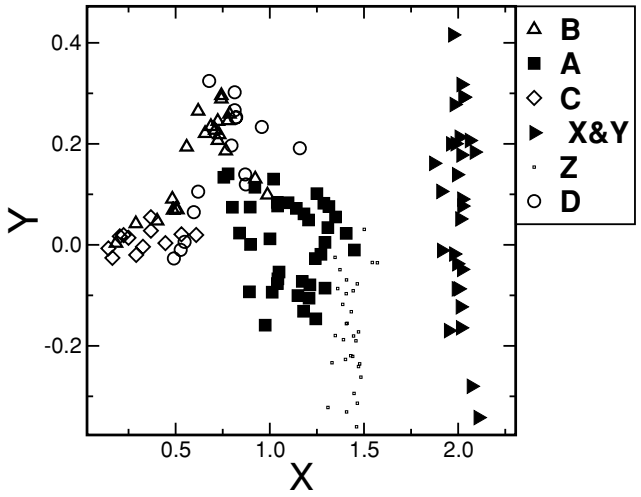


**Figure 8.** *X* versus *Y* coordinates of the identified jet components within 3-mas core separation are shown. This is to stress the fact that individual components like A, X and Y tend to populate certain parts of this diagram while others (like B and D) tend to move within this diagram. Based on this plot, we do not rule out that X and Y belong to the same jet component.

source similar to 4C39.25 has been found in the quasar 1338+381 by Bouchy et al. (1998).

We do not want to rule out the possibility that the three CAEs in S5 1803+784 might be caused by different physical mechanisms. Several scenarios to explain the observed first and second oscillation of jet component A are possible.

(i) The jet component identification is wrong: instead of identifying the brightest jet component as component A, we might have identified it (at times of smaller core separation) as the jet component approaching component A. It is also possible that we failed to model an additional component, which would easily explain the increasing major axis when A approaches the core (again a blending effect). However, Z shows similar behaviour to A, which makes this possibility less likely.

(ii) Blending of components unresolved by the interferometer beam at *X*-band: component A is a blend of several individual components that move (see Krichbaum et al. 1993).

(iii) Apparent shifts of the self-absorbed flat-spectrum VLBI core used as the fiducial reference in the images at each epoch: the apparent correlation of two of the minima of core separation observed for A and also evident for Z, coincident with the appearance of the components B in ∼1988.5 and C in ∼ 1990.5 (see Fig. 3) seems to support the hypothesis of a shift of the core position. If the core shifts due to blending effects caused by the emergence of new jet components, however, such position offsets must be visible for all components. This is not the case (i.e. components X and Y, which do not show similar CAEs).

(iv) The core is moving physically: this should then be detectable by phase reference observations, which have been carried out by Pérez-Torres et al. (2000). However, this would imply other problems because components X and Y are quite stable.

(v) Intrinsic motion: A moves in the rest frame of the source on an orbit perpendicular to the motion of the other jet components and thus approaches or separates from the core in the observer's frame. It is possible, that two sorts of jet components exist, moving 'normal' jet components that move on helical paths away from the core. In addition, A might represent a part of the jet, possibly bent towards us, where we see into the jet at a different angle.

Based on VLBI polarization observations (including the space telescope *HALCA*) at 5 and 1.6 GHz, 1803+784 reveals a smoothly bent jet structure, with the magnetic field transverse all along the jet (Gabuzda 2000), reflecting the toroidal component of a helical magnetic field associated with the VLBI jet of this source. We do not rule out the possibility, that the motion of A is caused by this field.

In the following chapter, we discuss the most likely mechanism to explain the third observed oscillation of A.

### 5.1 Reconfinement shocks

The following analysis is based on a simplified treatment of reconfinement shocks (R-shocks) in jets (Beckert et al., in preparation). The third 'event', between late 1989 and the beginning of 1992 can be understood according to Beckert et al. as a reaction of an R-shock (Sanders 1983) to changes in the kinetic jet power $Q$. In a hydrodynamics scenario of jet propagation, the jets can either be confined or unconfined by the pressure in the ambient medium. A jet, which starts out in pressure equilibrium with its surroundings, breaks free if the external pressure decreases more rapidly than $P_{\rm ex}^{(c)} \propto z^{-2}$ ($z$ is the distance from the origin of the jet along the jet axis). This situation can appear in Bondi-like accretion flows within the accretion radius of the central black hole. Beyond the accretion radius, the pressure gradient is expected to have a much larger scalelength. Hence, the pressure drops much more slowly and the jet will be reconfined. As a consequence, an R-shock forms inside the highly supersonic jet. The shock starts at the jet boundary at $z_0$ and extends to the jet axis where it terminates at $z_{\rm t}$. The expected shape of the R-shock is derived in Komissarov & Falle (1997). For a power-law pressure distribution $P = P_0(z/z_0)^{-\eta}$ in the ambient medium, the termination point is given by

$$z_{\rm t} = \left( z_0^{\delta} + \frac{\Theta\delta}{A} \right)^{1/\delta} \tag{1}$$

with the parameter

$$A = z_0^{(1-\delta)} \left( \frac{P_0 \Gamma_1 \pi \Theta^2}{\mu Q u_1} \right)^{1/2}, \tag{2}$$

where the exponent $\delta = 1 - \eta/2$ in equation (1) is related to the pressure gradient, $\Theta$ is the half-opening angle of the jet before the shock, $u_1$ is the pre-shock 4-velocity, $\Gamma_1$ the Lorentz factor of the bulk motion and $\mu \approx 17/24$ a constant according to Komissarov & Falle (1997).

Beckert et al. (in preparation) associate the emission region of stationary or quasi-stationary components with $z_{\rm t}$ when practically all jet material has passed the R-shock. For the reconfinement to be effective, the pressure gradient must be flatter than $\eta = 2$, which implies that $\delta$ is positive. In the following, we assume $\eta = 1.5$.

### 5.2 The motion of quasi-stationary jet components

According to equation (1), the position of the stationary R-shock, which we interpret as a jet component, depends on the parameter $A$. Secular changes of $A$ will lead to a motion of $z_{\rm t}$, which can be due to changes in the jet power $Q$. The stationary component (A) would approach the core for a decreasing $Q$ (see equation 2) and a further episode of increasing $Q$ could move the component outwards again. Beckert et al. (in preparation) perform simulations of the reaction

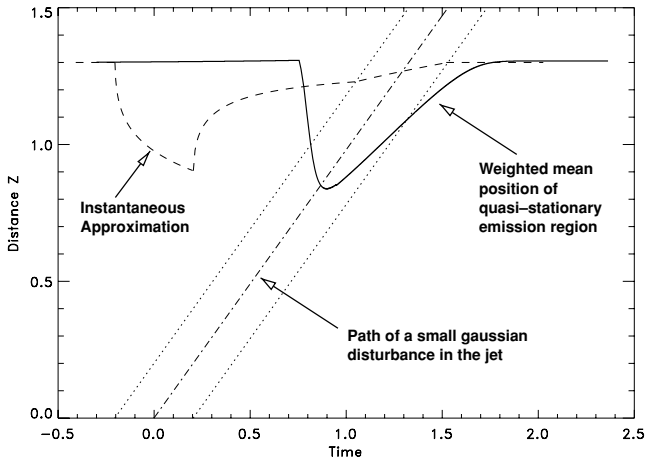


**Figure 9.** Interpolation of weighted mean position of component A. A weak disturbance with $\Delta Q = -0.15Q$ and large width $\delta z = 0.4$ travels along the jet. The bulk Lorentz factor of the jet is $\Gamma_l = 10$, which is also the velocity of the disturbance. During the time interval in which two shocks are present, the position moves quickly towards the core and travels outwards again in the wake of the disturbance.

of R-shocks to gaussian perturbations of $\Delta Q = -0.15Q$ travelling with $\Gamma = 10$ along the jet, taken to be the same as that of the jet flow. The projected width of the disturbance is 0.4 mas and is assumed to be constant. For a perturbation with sharp edges, an analytic instantaneous approximation is shown in Fig. 9, where it is assumed that the whole R-shock reacts instantaneously to the appearance of the perturbation. A new R-shock forms at a smaller distance, while the old R-shock survives and disappears when the information of the perturbation has reached the old $z_t$. Therefore, the reaction is delayed when compared to the instantaneous approximation and a weighted mean position for the component A as seen in Fig. 9 is used.

All motions associated with the reaction of R-shocks are changing patterns and the velocities of A in Fig. 3(a) are pattern speeds. In addition, the fast backward jump of A shown in Fig. 9 is a blending effect of two R-shocks, one fading and one newly appearing and taking over.

The theoretical model presented above quite nicely reproduces the observed third CAE. However, because the first two oscillation events show a significantly different signature, we can not rule out that other processes might be at work as well. Further insight might come from combining observations taken at different radio frequencies. For a more detailed treatment of a possible R-shock in 1803+784, we refer to Beckert et al. (in preparation).

## ACKNOWLEDGMENTS

We thank A. M. Gontier and W. Alef for useful discussions, and A. Mueskens for help exporting the VLBI data. This research has made use of data from the University of Michigan Radio Astronomy Observatory, which is supported by the National Science Foundation and by funds from the University of Michigan. We thank M. and H. Aller for communicating data prior to publication. Part of this work was supported by the European Commission, TMR Programme, Research Network Contract ERBFMRXCT97-0034 'CERES'. SB acknowledges support by the Claussen-Simon-Stiftung. This research has made use of the National Aeronautics and Space Administration (NASA) Infrared Processing and Analysis Center (IPAC) Extragalactic Database (NED), which is operated by the Jet Propulsion Laboratory, California Institute of Technology, under contract with NASA.

## REFERENCES

Agudo I., Gómez J. L., Martí J.-M., Ibáñez J.-M., Marscher A. P., Alberdi A., Aloy M.-A., Hardee P. E., 2001, ApJ, 549, L183
Alberdi A. et al., 1993a, A&A, 271, 93
Alberdi A., Marcaide J. M., Marscher A. P., Zhang Y. F., Elosegui P., Gómez J. L., Shaffer D. B., 1993b, ApJ, 402, 160
Alberdi A., Gómez J. L., Marcaide J. M., Marscher A. P., Pérez-Torres M. A., 2000, A&A, 361, 529
Antonucci R. R. J., Hickson P., Olszewski E. W., Miller J. S., 1986, AJ, 92, 1
Biermann P. L., Schaaf R., Pietsch W., Schmutzler T., Witzel A., Kühr H., 1992, A&AS, 96, 339
Bouchy F., Lestrade J.-F., Ransom R. R., Bartel N., Ratner M. I., Shapiro I. I., 1998, A&A, 335, 145
Britzen S., 1997, PhD thesis, Univ. Bonn
Britzen S., 2002, Rev. Mod. Astron., 15, 199
Britzen S., Krichbaum T. P., 1995, in Lanotte R., Bianco G., eds, Proc. 10th Working meeting on European VLBI for Geodesy and Astrometry. Agenzia Spaziale Italiano, Matera, p. 172
Britzen S., Witzel A., Krichbaum T. P., Qian S. J., Campbell R. M., 1999, A&A, 341, 418
Britzen S., Witzel A., Krichbaum T. P., Campbell R. M., Wagner S. J., Qian S. J., 2000, A&A, 360, 65
Britzen S. et al., 2005a, A&A, accepted
Britzen S. et al. 2005b, A&A, submitted
Cassaro P., Stanghellini C., Bondi M., Dallacasa D., della Ceca R., Zappalà R. A., 1999, A&AS, 139, 601
Cawthorne T. V., Wardle J. F. C., Roberts D. H., Gabuzda D. C., Brown L. F., 1993, ApJ, 416, 496
Charlot P., 1990a, AJ, 99, 1309
Charlot P., 1990b, A&A, 229, 51
Charlot P., 1992, J. Astronomes Francais, 43, 39
Eckart A., Witzel A., Biermann P., Johnston K. J., Simon R., Schalinski C., Kühr H., 1986, A&A, 168, 17
Eckart A., Witzel A., Biermann P., 1987, A&A, 67, 121
Fey A. L., Clegg A. W., Fomalont E. B., 1996, ApJS, 105, 299
Gabuzda D. C., 1999, New Astron. Rev., 43, 691
Gabuzda D. C., 2000, in Hirabayashi H., Edwards P. G., Murphy D. W., eds, Proc. VSOP Symp., Astrophysical phenomena revealed by space VLBI. Institute of Space and Astronautical Science, Sagamihara, Kanagawa, Japan, p. 121
Gabuzda D. C., Cawthorne T. V., 2000, MNRAS, 319, 1056
Gabuzda D. C., Wardle J. F. C., Roberts D. H., Aller M. F., Aller H. D., 1994, ApJ, 435, 128
Homan D. C., Ojha R., Wardle J. F. C., Roberts D. H., Aller M. F., Aller H. D., Hughes P. A., 2002, ApJ 568, 99
Kellermann K. I., Vermeulen R. C., Zensus J. A., 1998, AJ, 115, 1295
Komissarov S. S., Falle S. A. E. G., 1997, MNRAS, 288, 833
Krichbaum T. P., 1990, in Zensus J. A., Pearson T. J., eds, Parsec-scale Radio Jets. Cambridge Univ. Press, Cambridge, p. 83
Krichbaum T. P., Witzel A., Graham D. A., Schalinski C. J., Zensus J. A., 1993, in Davies R. J., Booth R. S., eds, Subarcsecond Radio Astronomy. Cambridge Univ. Press, Cambridge, p. 181
Krichbaum T. P., Standke K. J., Graham D. A., Witzel A., Schalinski C. J., Zensus J. A., 1994a, in Courvoisier T. J.-L., Blecha A., eds, Proc. IAU Symp. 159, Multi-wavelength continuum emission of AGN. Kluwer, Dordrecht, p. 187
Krichbaum T. P., Witzel A., Standke K. J., Graham D. A., Schalinski C. J., Zensus J. A., 1994b, in Zensus J. A., Kellermann K. I., eds, Proc. 1994 NRAO Workshop No. 23, Compact Extragalactic Radio Sources. NRAO, Green Bank, p. 39

Lawrence C. R., Zucker J. R., Readhead A. C. S., Unwin S. C., Pearson T. J., Xu W., 1986, ApJS, 107, 541
Marcaide J. M., Alberdi A., Elosegui P., Schalinski C. J., Jackson N., Witzel A., 1989, A&A, 211, 23
Pearson T. J., 1991, BAAS, 23, 991
Pérez-Torres M. A., Marcaide J. M., Guirado J. C., Ros E., Shapiro I. I., Ratner M. I., Sardón E., 2000, A&A, 360, 161
Ros E., Marcaide J. M., Guirado J. C., Sardón E., Shapiro I. I., 2000, A&A, 356, 357
Ros E., Marcaide J. M., Guirado J. C., Pérez-Torres M. A., 2001, A&A, 376, 1090
Sanders R. H., 1983, ApJ, 266, 73
Schalinski C. J., 1985, Diploma thesis, Univ. Bonn
Schalinski C. J., 1990, Dissertation, Universität Bonn, Bonn
Schalinski C. J., Alef W., Witzel A., Campbell J., Schuh H., 1988a, in Reid M. J., Moran J. M., eds, Proc. IAU Symp. 129, The impact of VLBI on astrophysics and geophysics. Kluwer, Dordrecht, p. 359
Schalinski C. J., Witzel A., Krichbaum T. P., Hummel C. A., Biermann P. L., Johnston K. J., Simon R. S., 1988b, in Reid M. J., Moran J. M., eds, Proc. IAU Symp. 129, The impact of VLBI on astrophysics and geophysics. Kluwer, Dordrecht, p. 71
Schuh H., 1989, IEEE Trans. Instrum. Meas., 38, 676
Simon R. S., Hall J., Johnston K. J., Spencer J. H., Waak J. A., Mutel R. L., 1988, ApJ, 326, 5
Spergel D. N. et al., 2003, ApJS, 148, 175
Steffen W., 1997, Vistas Astron., 41, 71
Steffen W., Krichbaum T. P., Britzen S., Witzel A., 1995, in Green D. A., Steffen W., eds, The XXVIIth Young European Radio Astronomers Conference, Cambridge Univ. Press, Cambridge, p. 29
Stickel M., Fried J. W., Kühr H., 1993, A&AS, 98, 393
Tang G., Rönnäng B., 1988, in Reid M. J., Moran J. M., eds, Proc. IAU Symp. 129, The impact of VLBI on astrophysics and geophysics. Kluwer, Dordrecht, p. 431
Tang G., Rönnäng B., Baath L., 1987, A&A, 185, 87
Tang G., Rönnäng B., Baath L., 1989, A&A, 216, 31
Tateyama C. E., Kingham K. A., Kaufmann P., de Lucena A. M. P., 2002, ApJ, 573, 496
Ulvestad J. S., 1988, in Reid M. J., Moran J. M., eds, Proc. IAU Symp. 129, The impact of VLBI on astrophysics and geophysics. Kluwer, Dordrecht, p. 429
Wagner S. J., Witzel A., 1995, ARA&A, 33, 163
Wagner S. J., Sanchez-Pons F., Quirrenbach A., Witzel A., 1990, A&A, 235, L1
Witzel A., 1987, in Zensus J. A., Pearson T. J., eds, Superluminal Radio Sources. Cambridge Univ. Press, Cambridge, p. 83
Witzel A., Schalinski C. J., Johnston K. J., Biermann P. L., Krichbaum T. P., Hummel C. A., Eckart A., 1988, A&A, 206, 245
Zensus J. A., 1997, ARA&A, 35, 607

This paper has been typeset from a TEX/LATEX file prepared by the author.